ORGANOMETALLICS

pubs.acs.org/Organometallics

Article

Co(cyclam) Complexes of Triarylamine-acetylide: Structural and Spectroscopic Properties and DFT Analysis

Susannah D. Banziger, Adharsh Raghavan, Matthias Zeller, and Tong Ren*

Cite This: *Organometallics* 2020, 39, 3250–3259

Read Online

ACCESS | Metrics & More | Article Recommendations | Supporting Information

ABSTRACT: Reported herein are the syntheses of mono- and bis-C_2TPA (HC_2TPA = 4-ethynyl-*N*,*N*-bis(4-methoxyphenyl)aniline) complexes of Co^{III}(cyclam) (cyclam = 1,4,8,11-tetraazacyclotetradecane) complexes, and the formation of η^2-adducts of Cu(I)/Ag(I) to the acetylenic bond of $TPAC_2$ ligand. The reaction between *trans*-[Co(cyclam)Cl_2]Cl and HC_2TPA in the presence of Et_2NH yielded *trans*-[Co(cyclam)(C_2TPA)Cl]Cl ([**1**]Cl) and subsequent treatment of [**1**]Cl with CuCl or $AgNO_3$ afforded *trans*-[Co(cyclam)(C_2TPA-η^2-$CuCl_2$)Cl] (**2a**) or *trans*-[Co(cyclam)(C_2TPA-η^2-Ag$(NO_3)_2$)(NO_3)] (**2b**), respectively. The reaction between [Co(cyclam)Cl_2]Cl and 3 equiv of LiC_2TPA afforded *trans*-[Co(cyclam)$(C_2TPA)_2$]Cl ([**3**]Cl). X-ray diffraction studies of compounds [**1**]Cl, **2a**/**b**, and [**3**]Cl established their molecular structures. All four compounds display redox couples that are characteristic of TPA (reversible oxidation) and Co^{III} (irreversible reduction) center. The reversible TPA oxidation in compounds [**1**]Cl and [**3**]Cl enables further UV−vis/near-IR spectroelectrochemical studies to elucidate the change of electronic structures upon oxidation. The electronic spectra of both compounds [**1**]Cl and [**3**]Cl and their oxidized derivatives have been rationalized based on DFT and TD-DFT analysis.

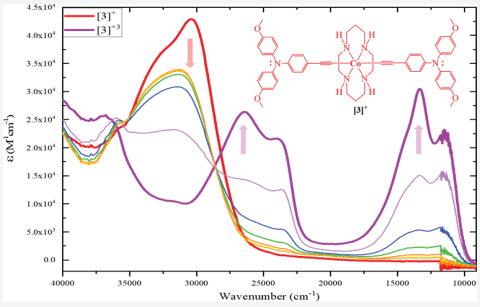

INTRODUCTION

The chemistry of transition metal alkynyls has evolved extensively since the early study of homoleptic complexes $[M(C{\equiv}CR)_m]^{n-}$ by Nast and co-workers.[1] In addition to continuous interest in new synthesis[2−4] and understanding of structures and bonding of metal alkynyls,[5−7] recent decades have witnessed significant progress in areas such as molecular electronic wires and devices[8−13] and optoelectronic materials.[14] One of the peculiar attributes of metal alkynyl complexes is the propensity to form an η^2-adduct of Cu(I)/Ag(I) at the acetylenic unit that bonds to the metal center (Chart 1),[15] and it has been demonstrated that the η^2-coordination of Cu(I) attenuates the electronic coupling between two Ru(II) centers linked by butadiynyl.[16]

Chart 1. Metal (M) σ-Alkynyl with η^2 Coinage Metal (M′) Adduct

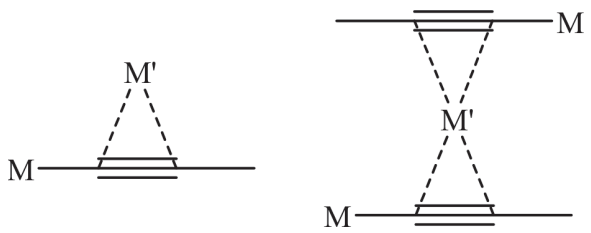

Our laboratory has become interested in 3d metal alkynyl compounds supported by both cyclam (1,4,8,11-tetraazacyclotetradecane) and its C-substituted derivatives.[17,18] Though the area is fairly young, Co(cyclam)-based compounds have been a frequent target due to the possibility of high yield preparation of *trans*-[Co(cyclam)(C_2R)Cl]$^+$ under mild conditions.[19−21] Recent efforts led to the preparation of [Co(cyclam)-(C_2NAP^R)Cl]Cl (NAP^R = *N*-R-1,8-naphthalimide with R as isopropyl, NAP^{iPr}, and mesityl, NAP^{Mes}) with a focus on the NAP^R moiety as an emissive electron acceptor.[22,23] Explored in this study are the [Co(cyclam)(C_2TPA)Cl]$^+$ and [Co-(cyclam)$(C_2TPA)_2$]$^+$ type compounds with HC_2TPA as 4-ethynyl-*N*,*N*-bis(4-methoxyphenyl)aniline. Triarylamines (Ar_3N) are excellent electron donors and exhibit a reversible one-electron oxidation that is accompanied by drastic changes in electronic absorption spectra, the latter of which has been frequently exploited in probing both organic[24−26] and organometallic mixed valency through spectroelectrochemical investigation.[27] Hence, a key focus of the current study is the spectral response of the Co compounds upon the oxidation of

Received: July 6, 2020
Published: August 25, 2020

https://dx.doi.org/10.1021/acs.organomet.0c00454
Organometallics 2020, 39, 3250−3259

Scheme 1. Synthesis of Compounds [1]Cl, 2a, and 2b[a]

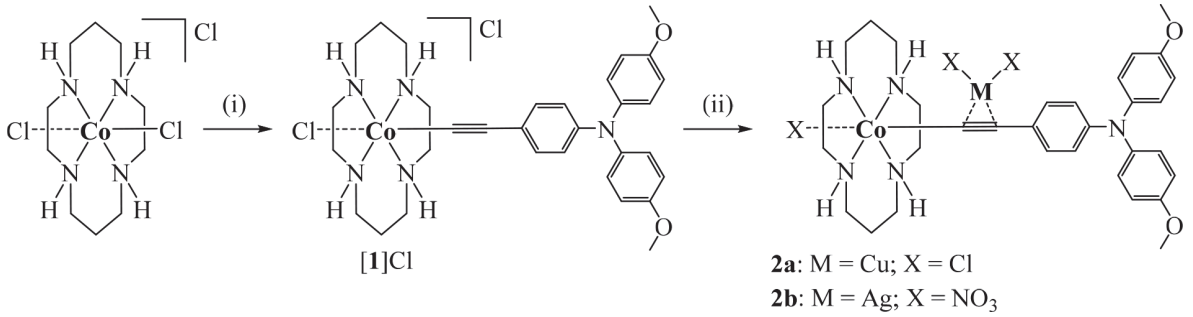

[a]Conditions: (i) HC_2TPA; Et_2NH, MeOH/THF; 60 °C, 12 h; (ii) [1]Cl, M−X, MeOH/MeCN; 60 °C, 4−12 h.

TPA and theoretical insight based on TD-DFT analysis. In addition, *trans*-[Co(cyclam)(C_2TPA)Cl]$^+$ species readily form an η^2-adduct of Cu(I)/Ag(I), which is unique for Co-alkynyl species.

RESULTS AND DISCUSSION

Synthesis. As shown in Scheme 1, [Co(cyclam)(C_2TPA)Cl]Cl ([**1**]Cl) was prepared under weak base conditions[19] from the reaction between [Co(cyclam)Cl_2]Cl and HC_2TPA in a MeOH/THF/Et_2NH solution and isolated as a pink crystalline solid (75% yield). The synthesis of [Co(cyclam)-(C_2TPA-η^2-$CuCl_2$)Cl] (**2a**) was achieved via reflux of [**1**]Cl and CuCl in MeCN for 12 h in 74% yield. [Co(cyclam)-(C_2TPA-η^2-$Ag(NO_3)_2$)(NO_3)] (**2b**) was prepared similarly from [**1**]Cl and $AgNO_3$ and isolated as a dark red solid in 70% yield. Attempts to synthesize [Co(cyclam)(C_2TPA-η^2-Ag-$(Cl)_2$)Cl] proved futile due to the low solubility of AgCl. Furthermore, compound **2b** exhibited extremely low solubility, preventing the study of physical properties such as absorption spectra and voltammetry. [Co(cyclam)(C_2TPA)$_2$]Cl ([**3**]Cl) was prepared from the reaction of [Co(cyclam)Cl_2]Cl with 3 equiv of LiC_2TPA in THF. After silica gel plug purification, compound [**3**]Cl was isolated as a light brown solid in 84% yield. Attempts to react CuCl or $AgNO_3$ with [**3**]Cl to form η^2-MX_2 type species (M = Cu or Ag; X = Cl or NO_3) resulted in formation of an insoluble yellow solid that could not be further analyzed. All compounds presented herein are low spin Co(III) species and are readily characterized using ^{1}H NMR, UV−vis−NIR, and FT-IR spectroscopies, ESI mass spectrometry, and combustion analysis.

Structure Analysis. Single crystals of [**1**]Cl, **2a**, **2b**, and [**3**]Cl were grown from slow diffusion of diethyl ether into a concentrated solution of the respective compound. Molecular structures of [**1**]$^+$ (Figure 1), **2a** (Figure 2), **2b** (Figure 3), and [**3**]$^+$ (Figure 4) were determined using single crystal X-ray diffraction. In all structures, the Co center adopts a pseudo-octahedral geometry with the alkynyl and chloro ligands in the axial positions trans to each other. No additional counterion was observed for **2a** and **2b**, suggesting that Cu(I) and Ag(I) were coordinated, respectively. Selected bond lengths and angles can be found in Table 1, and the details of data collection and structure refinement can be found in the Table S1.

The C≡C and Co−C bond lengths for [**1**]$^+$ and [**3**]$^+$ follow the canonical trend for mono- versus symmetric bis-Co^{III}(cyclam) acetylides,[17,18] in which the C≡C bond lengths are identical within the experimental errors and the Co−C bond in [**1**]$^+$ (1.879(3) Å) is shorter than that in [**3**]$^+$

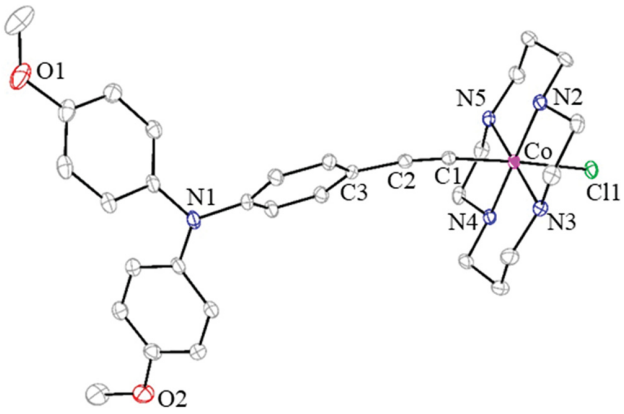

Figure 1. ORTEP plot of [**1**]$^+$ at 30% probability level. Hydrogen atoms, solvent molecules, and the counterion are omitted for clarity.

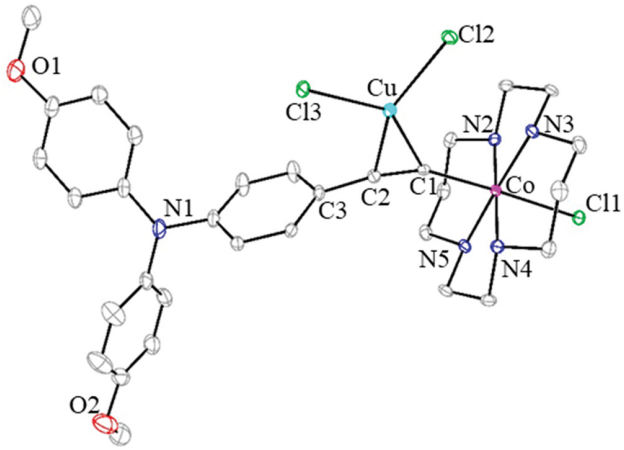

Figure 2. ORTEP plot of **2a** at 30% probability level. Hydrogen atoms and solvent molecules are omitted for clarity.

(1.945(2) Å) due to the trans influence in the latter.[28] The Co−C bond lengths are also comparable to those observed for analogous Co^{III}(cyclam) species with electron-rich acetylides, [Co(cyclam)($C_2C_6H_4$-4-NMe_2)(NCMe)]$^+$ (1.874(2) Å) and [Co(cyclam)($C_2C_6H_4$-4-NMe_2)$_2$]$^+$ (1.942(3) Å).[21,29]

Comparison of [**1**]$^+$ to **2a** and **2b** reveals that the $\eta^2(\pi)$-coordination of MX_2 to the acetylide has resulted in an appreciable elongation of the Co−C, C≡C, and C2−C3 bonds (Table 1). Chen and co-workers also noted the elongation of Ru−C and C≡C bonds for Ru−C≡C−C≡

https://dx.doi.org/10.1021/acs.organomet.0c00454
Organometallics 2020, 39, 3250−3259

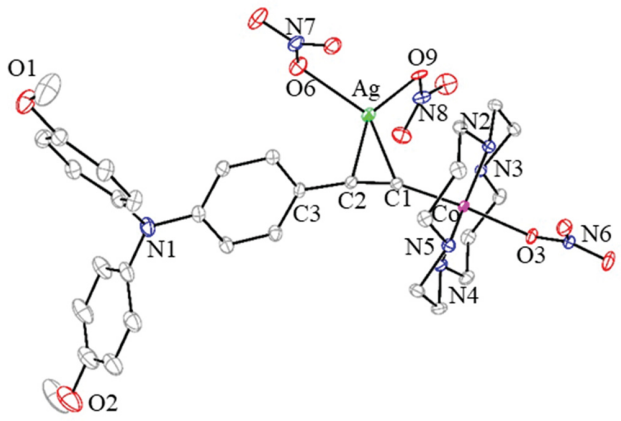

Figure 3. ORTEP plot of **2b** at 30% probability level. Hydrogen atoms, solvent molecules, and disorder are omitted for clarity.

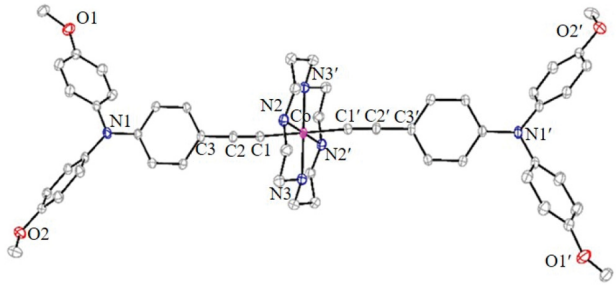

Figure 4. ORTEP plot of $[3]^+$ at 30% probability level. Hydrogen atoms and the counterion are omitted for clarity.

C−Ru systems when the alkynes were η^2 coordinated to Cu(I).[16] The Cu−C bond lengths (average 2.027[2] Å) were consistent with literature reports for a Cu(I) species,[16] as were the Ag−C bond lengths (average 2.318[5] Å) for a Ag(I) species.[30] Compared to $[1]^+$ (Figure S1), significant curvature due to the nonlinearity of the Co−C1−C2 and C1−C2−C3 bonds were noted for compounds **2a** and **2b** and were attributed to η^2-coordination of Cu(I) and Ag(I), respectively. Similar distortions were noted for Pt−C≡C− polymers coordinated by Cu_2Y_2 (Y = I, Br, or Cl) in which the Cu-coordinated species had longer C≡C bonds and bent C−C≡C bonds.[31]

Fourier Transform Infrared Spectra (FTIR). The ATR-FTIR spectra shown in Figure 5 highlight the C≡C stretching

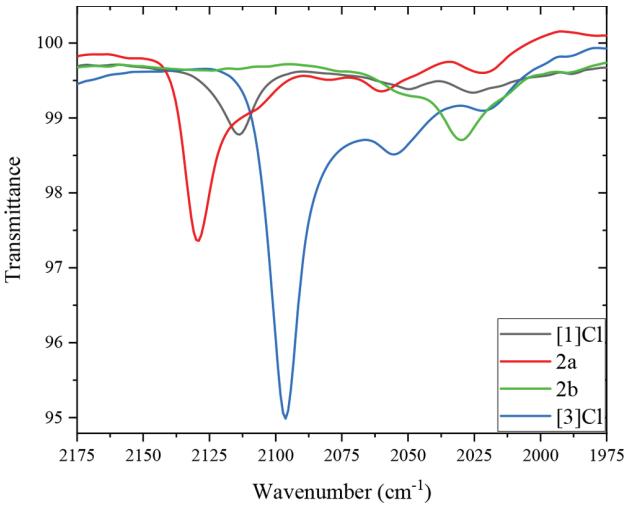

Figure 5. ATR-FTIR of [**1**]Cl, **2a**, **2b**, and [**3**]Cl highlighting the C≡C stretches.

frequencies for [**1**]Cl, **2a**, **2b**, and [**3**]Cl. Consistent with previous work,[21,22] ν(C≡C) of compound [**3**]Cl is lower than that of [**1**]Cl due to the presence of a second alkynyl ligand in place of a chloro ligand in the trans position, which results in greater antibonding interactions between Co dπ and filled π(C≡C) orbitals and hence weakened C≡C bonds.[28] In agreement with the experimentally observed structure data, compound **2b** (1.234(4) Å; 2030 cm^{-1}) has a longer C≡C bond and a lower ν(C≡C) compared to those of [**1**]Cl (1.205(4) Å; 2114 cm^{-1}). However, compound **2a** does not follow this expected trend, with a C≡C bond length of 1.232(3) Å and ν(C≡C) of 2129 cm^{-1}. This experimental anomaly could be attributed to a number of factors such as (i) the lighter atomic mass of Cu(I) (compared to Ag(I)) and (ii)

Table 1. Selected Bond Lengths (Å) and Bond Angles (deg) for $[1]^+$, 2a, 2b, and $[3]^+$

	$[1]^+$	2a	2b	$[3]^+$
Co−N2	1.969(2)	1.980(2)	1.962(2)	1.992(2)
Co1−N3	1.975(2)	1.984(2)	1.982(2)	1.987(2)
Co1−N4	1.976(2)	1.975(2)	1.983(2)	
Co1−N5	1.980(2)	1.972(2)	1.968(2)	
Co1−C1	1.879(3)	1.928(2)	1.891(3)	1.945(2)
Co1−Cl1/O3/C1′	2.3401(7)	2.3228(6)	1.984(2)	1.945(2)
Cu/Ag−C1		2.011(2)	2.317(2)	
Cu/Ag−C2		2.042(2)	2.319(3)	
Cu−Cl2/Ag−O6		2.2670(6)	2.33(2)	
Cu−Cl3/Ag−O7		2.2728(6)	2.382(2)	
C1−C2	1.205(4)	1.232(3)	1.234(4)	1.203(3)
C2−C3	1.434(4)	1.450(3)	1.442(3)	1.446(3)
Cl/O3/C1′−Co1−C1	177.26(8)	177.23(6)	172.99(9)	180.0
Co1−C1−C2	172.6(2)	153.5(2)	158.5(2)	175.8(2)
C1−C2−C3	171.6(3)	165.8(2)	167.3(3)	177.5(3)
C1−Cu/Ag−C2		35.37(8)	30.89(9)	
Co1−C1−C2−C3		18.4(12)	−2.0(17)	

https://dx.doi.org/10.1021/acs.organomet.0c00454
Organometallics 2020, 39, 3250−3259

the relative π-donor character of the atom *trans* to the acetylide ligand. Since the spectra were recorded on pure solids, the dissociation of Cu(I)/Ag(I), a plausible solution process, is not a contributing factor. The nitrato ligand (**2b**) is a better π-acceptor than the chloro (**2a**) and could influence the ν(C≡C) more than the η^2-coordinated metal.[32]

UV−Vis and Florescent Spectroscopic Analysis. Absorption spectra for compounds [**1**]Cl, **2a**, and [**3**]Cl were collected at room temperature in both CH_2Cl_2 and MeCN under ambient conditions. Emission spectra for compounds [**1**]Cl and [**3**]Cl were collected at room temperature in CH_2Cl_2. Table 2 lists absorption (λ_{abs}) and emission maxima (λ_{em}) in CH_2Cl_2. While the absorption spectra recorded in CH_2Cl_2 and MeCN are very similar, emission was not detected in MeCN. The solubility of compound **2b** was too low to yield quality spectroscopic (Figure S2) and voltammetric information, and these properties will not be discussed further. As shown in Figure 6,

Table 2. Absorption (λ_{abs}) and Emission Maxima (λ_{em}, nm), Excitation Wavelength (λ_{ex}, nm), and Emission Quantum Yields (Φ_{fl}) in CH_2Cl_2 at Room Temperature

	Φ_{fl}	λ_{abs}	λ_{em}	λ_{ex}
$TPAC_2H$	0.11	301	460	301
[**1**]Cl	0.00058	327	459	305
[**3**]Cl	0.018	333	462	305

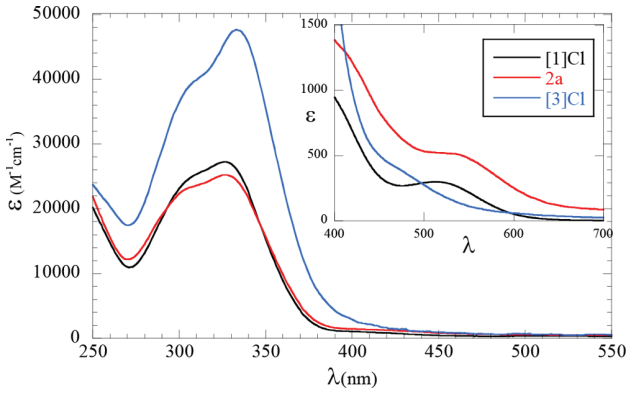

Figure 6. Absorption spectra of [**1**]Cl, **2a**, and [**3**]Cl in CH_2Cl_2

compounds [**1**]Cl, **2a**, and [**3**]Cl display a strong absorption band at ca. 330 nm with an extinction coefficient around 48 000 M^{-1} cm^{-1} for [**3**]Cl and ∼25 000 M^{-1} cm^{-1} for compounds [**1**]Cl and **2a**. Both the peak positions and intensities are very close to those of the $(p\text{-}YC_6H_4)_3N$ (Y = Cl, CH_3, or OCH_3) series studied by Lambert,[33] suggesting this transition is dominated by the $\pi \rightarrow \pi^*$ transition of the TPA moiety. Furthermore, both inorganic and organic compounds containing triaryl amine functional group, such as Ru(II)[34] and Co(II) complexes[35] with a distal TPA pendant, $(TPA)_2(\mu\text{-}C_4)$,[36] and diruthenium bridged by TPA-diethynyl,[37] exhibit similar intense TPA-based $\pi \rightarrow \pi^*$ transitions under 400 nm, illustrating the metal-independence of the TPA chromophore. Though the broad nature of this peak partially obscures the d−d ($^1A_{1g} \rightarrow {}^1T_{1g}$, O_h) band in [**3**]Cl, the d−d band is easily identifiable for compounds [**1**]Cl and **2a** (inset of Figure 6) with peak positions comparable to those of previously reported Co^{III}(cyclam) monoacetylides.[20,22,28,29,38] Especially noteworthy is the similarity in peak positions and extinction coefficients for compounds [**1**]Cl and **2a**, suggesting that η^2-coordination by Cu(I) has a minimal effect on the electronic structures of compounds **2**.

Steady-state emission spectra of compounds [**1**]Cl and [**3**]Cl were recorded, and the emission data are collected in Table 2. The spectra are provided in the Figure S3. Compounds **2a** and **2b** are nonemissive under similar experimental conditions, pointing to the quencher role of Cu(I)/Ag(I) centers. The emission profiles of compounds [**1**]Cl and [**3**]Cl are very similar to that of the $TPAC_2H$, clearly indicating an origin of $S_0 \rightarrow S_1$ excitation of the TPA moiety.[36,39] Consistent with previous reports of Co^{III}(cyclam) alkynyl species bearing simple chromophores such as naphthalene[38] and naphthalimide,[22] the Co(III) center greatly reduces the emission quantum yield of the fluorophore. Compound [**3**]Cl (1.8%) has a Φ_{fl} significantly higher than that of compound [**1**]Cl (0.058%), due to the presence of two TPA ligands.

Electrochemistry. Compounds [**1**]Cl, **2a**, and [**3**]Cl were studied electrochemically and their cyclic voltammograms (CVs) are shown in Figure 7. The respective redox potentials

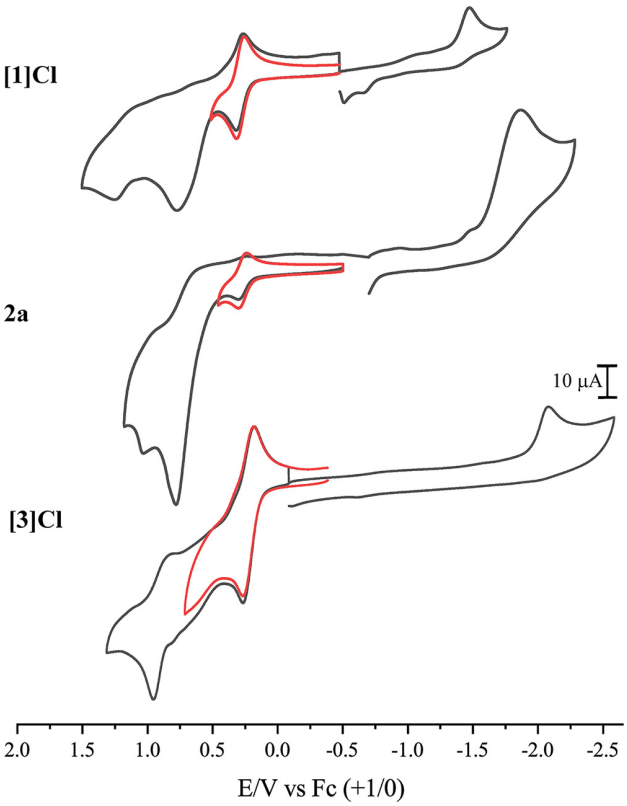

Figure 7. Cyclic voltammogram of a 1.0 mM solution of [**1**]Cl, **2a**, and [**3**]Cl in a 0.1 M solution of *n*-Bu_4NPF_6 in MeCN at scan rate = 0.1 V/s.

(all potential data in the ensuing discussion are referenced to an *external* ferrocene standard) listed in Table 3. Within the solvent window, Co^{3+} undergoes one irreversible 1e$^-$ reduction ($Co^{3+/2+}$) and one irreversible 1e$^-$ oxidation ($Co^{4+/3+}$). Although a second irreversible 1e$^-$ reduction ($Co^{2+/1+}$) was observed in previous studies of Co^{III}(cyclam) alkynyl complexes,[17,18,20−22] the electron-donating C_2TPA ligand cathodically shifts the $Co^{2+/1+}$ couple to beyond the solvent

https://dx.doi.org/10.1021/acs.organomet.0c00454
Organometallics 2020, 39, 3250−3259

Table 3. Electrode Potentials of All Observed Redox Couples (V) in TPA-Br, [1]Cl, 2a, and [3]Cl[a]

	$E_{1/2}(TPA^{+1/0})$	$E_{1/2}(TPA^{+2/+1})$	$E_{pa}(Co^{4+/3+})$	$E_{pc}(Co^{3+/2+})$
TPA-Br[b]	0.29 (0.08)	0.98 (0.07)		
[1]Cl[c]	0.27 (0.06)	1.20 (0.10)	0.77	−1.55
2a[c]	0.28 (0.07)	1.05	0.82	−1.90
[3]Cl[c]	0.28 (0.08)	0.94 (0.10)	0.77	−2.03

[a]Electrode potentials vs Fc^+/Fc with peak separation (ΔE_p) for reversible processes shown in brackets. Solutions contain 1.0 mM analyte and 0.1 M n-Bu_4NPF_6 as the supporting electrolyte. [b]Collected in CH_2Cl_2. [c]Collected in MeCN solutions.

window. This is consistent with systems containing a similar anilino donor studied in MeCN, in which the ($Co^{3+/2+}$) event occurred at the edge of the solvent window for both $[Co(cyclam)(C_2C_6H_4\text{-}4\text{-}NMe_2)_2]^+$ (−2.08 V) and $[Co(cyclam)(C_2C_6H_4\text{-}4\text{-}NMe_2)(C_2C_6F_5)]^+$ (−1.86 V).[29] All three compounds exhibit two characteristic oxidations attributed to the TPA ligand (Table 3), the first is a reversible ([1]Cl and [3]Cl)/quasi-reversible (2a) oxidation occurring at ∼0.28 V ($TPA^{+1/0}$) and subsequently a quasi-reversible ([1]Cl and [3]Cl)/irreversible (2a) oxidation at ∼1.0 V ($TPA^{+2/+1}$). Redox couples measured in CH_2Cl_2 for TPA-Br occur at 0.29 V (1e⁻) and 0.98 V (1e⁻). Literature examples reported a reversible 1e⁻ oxidation at 0.29 V for TPA-Cl,[33] two reversible 1 e⁻ oxidations at 0.11 and 0.86 V for TPA-OMe,[33] and a reversible 2e⁻ oxidation at 0.30 V for $TPAC_4TPA$.[36] While the CVs indicate high stability of TPA cation(s) in both [1]Cl and [3]Cl, no attempt was made to isolate the TPA cation derivatives.

Comparison of the CVs for [1]Cl and 2a demonstrates that η^2-bonding of Cu(I) to −C≡C−TPA clearly has an impact on the electronic interactions within the system. Compared to [1]Cl, the Co oxidation in 2a is anodically shifted by 0.05 V, and the Co reduction is cathodically shifted by 0.35 V along with a significant increase in current. The former is likely due to an overlapping oxidation event based on $[CuCl_2]^-$, and the latter is due to increased electron density on Co provided by η^2-coordination of $[CuCl_2]^-$ to the alkyne, moving the Co reduction to more negative potentials. Moreover, the current of the $TPA^{+1/0}$ couple in 2a is substantially less than that in [1]Cl, while its $E_{1/2}$ remains the same. The latter is surprising since the η^2-coordination of Cu(I) should lead to an anodic shift. We surmise that complex 2a partially dissociates Cu(I) under electrochemical conditions, and the reversible $TPA^{+1/0}$ couple originates from the Cu-free species, while the $TPA^{+1/0}$ couple of the Cu-bound species becomes lumped with the large peak at ca. 900 mV. Alteration of redox behavior due to η^2-Cu(I) coordination was demonstrated for $[Cp(dppf)Ru]_2(\mu\text{-}C{\equiv}C{-}C{\equiv}C)$ (dppf = 1,1′-bis(diphenylphosphino)-ferrocene) type complexes: While reversible stepwise Ru-centered 1e⁻ oxidations were observed for this compound due to strong Ru−Ru coupling, these couples became irreversible upon Cu(I) coordination.[16] Comparison of the TPA oxidation peak current of [1]Cl to symmetric bis-alkynyl species [3]Cl suggests that [3]Cl undergoes a reversible 2e⁻ oxidation ($TPA^{+1/0}$) and a quasi-reversible 2e⁻ oxidation ($TPA^{+2/+1}$), implying the concurrent oxidation of both TPA units in [3]Cl; hence, the absence of discernible electronic coupling between them.

Spectroelectrochemistry. UV−vis−NIR spectroelectrochemistry was performed in an optically transparent thin-layer electrochemical (OTTLE) cell[40] with a CaF_2 window and a path length of 0.2 mm. CVs of compounds [1]Cl and [3]Cl were taken in the OTTLE cell and used to determine the location of the first oxidation event (0.88 V for both species vs Ag reference). On the basis of CV data listed above, it was estimated to be a 1e⁻ event for compound [1]Cl ([1]Cl → $\{[1]Cl\}^+$) and a 2e⁻ event for compound [3]Cl ([3]Cl → $\{[3]Cl\}^{+2}$). Spectroelectrochemical study of 2a was not pursued due to its poor redox stability.

Spectroelectrochemical data for [1]Cl (Figure 8) shows that upon oxidation the $\pi \rightarrow \pi^*$ (TPA) transition (330 nm, 30 000 cm⁻¹) is significantly weakened, and new transitions grow in around 25 000 cm⁻¹ (400 nm) and 12 500 cm⁻¹ (800 nm). These transitions are highly reminiscent in shape, and λ_{max} of literature examples that claim to undergo MLCT and LMCT between metal center and ligand, like Ru^{II}(TPA) species[34] and Fc-TPA species.[27] For $\{[3]Cl\}^{+2}$ (Figure 9), the NIR peaks at 13 000 and 11 000 cm⁻¹ are in similar positions to the peaks observed for the dication of tetraphenyl-*p*-phenylenediamine, which were attributed to the localized radical cation.[24,41] The natures of these electronic transitions have been investigated using TD DFT calculations (see below). In both cases, the

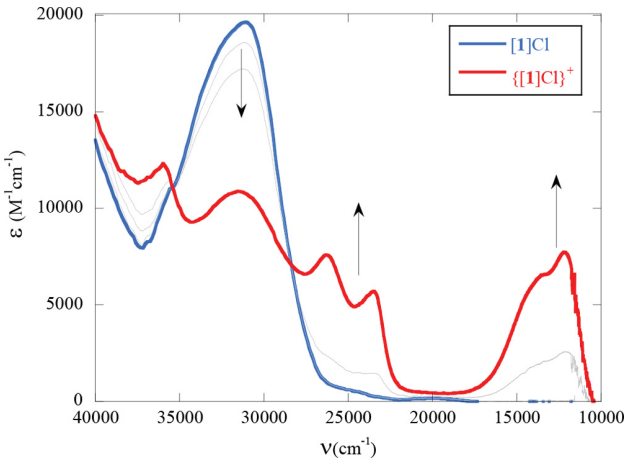

Figure 8. Absorption spectra in MeCN of [1]Cl in the neutral (blue) and 1e⁻-oxidized (red) states.

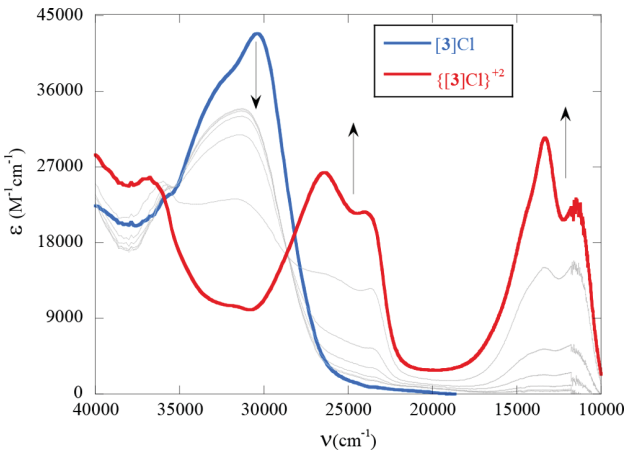

Figure 9. Absorption spectra in MeCN of [3]Cl in the neutral (blue) and 2e⁻-oxidized (red) states.

https://dx.doi.org/10.1021/acs.organomet.0c00454
Organometallics 2020, 39, 3250−3259

Table 4. Molecular Orbital Diagrams[a]

	$[1]^{+}$	$[1]^{+2}$ (alpha)	$[3]^{+}$	$[3]^{+3}$ (alpha)
LUMO+2	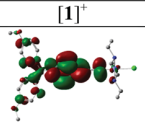 (−0.61)	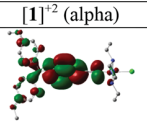 (−1.46)	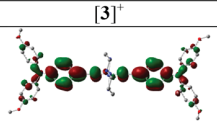 (−0.56)	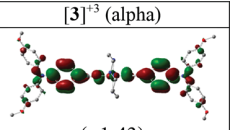 (−1.43)
LUMO+1	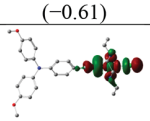 (−1.66)	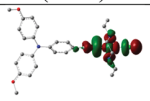 (−1.87)	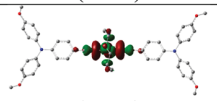 (−0.83)	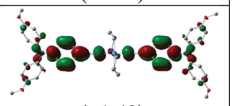 (−1.49)
LUMO	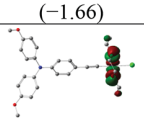 (−1.74)	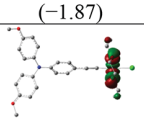 (−1.94)	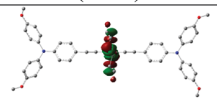 (−1.52)	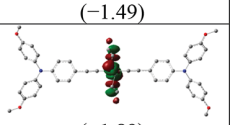 (−1.89)
HOMO/ SOMO[a]	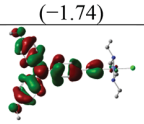 (−5.17)	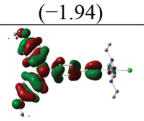 (−6.07)	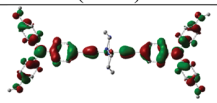 (−5.10)	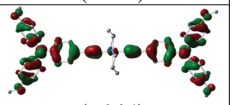 (−6.04)
HOMO−1	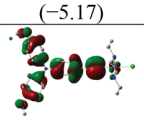 (−6.48)	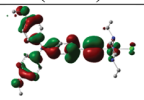 (−7.08)	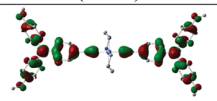 (−5.14)	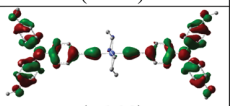 (−6.08)
HOMO−2	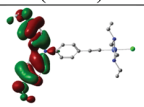 (−6.63)	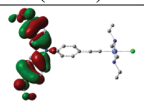 (−7.30)	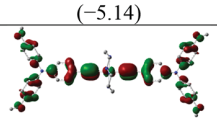 (−6.42)	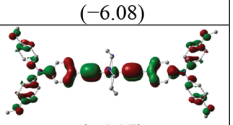 (−6.97)
HOMO−3	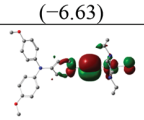 (−7.19)	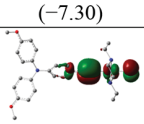 (−7.56)	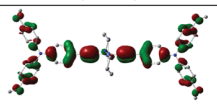 (−6.43)	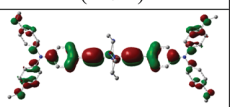 (−7.12)

[a]Plotted at lisovaluel = 0.025 and corresponding orbital energies (in eV) for $[1]^{+}$, $[1]^{+2}$, $[3]^{+}$, and $[3]^{+3}$ from DFT calculations. SOMO = singly occupied MO.

emerging peaks in the vis−NIR region are broad and clearly the results of overlapping peaks, which were deconvoluted using Gaussian fit peak analysis (Table S2, Figures S4 and S5).

Density Functional Theory (DFT) Calculations. To better understand the electronic structure of these compounds, DFT calculations were carried out on $[1]^{+}$, $[1]^{+2}$, $[3]^{+}$, and $[3]^{+3}$. The frontier molecular orbitals and corresponding energies are given in Table 4, and the comparison between experimental and DFT-optimized metrical parameters is given in Table S3. Computational details can be found in the Supporting Information.

It is clear from Table 4 that the frontier molecular orbitals are predominantly composed of the π system of the −C≡C− TPA unit with minimal contribution from the d-orbitals of Co. As suggested by the voltammetric analyses above, the HOMO of [1]Cl and [3]Cl are indeed based on the TPA moiety with a sizable contribution from the TPA-amino nitrogen lone pair. Therefore, the first oxidation event ($1e^{-}$ event in the case of $[1]^{+}$ and $2e^{-}$ event in the case of $[3]^{+}$) that occurs in these complexes gives rise to a $TPA^{\bullet+}$ radical cation, namely, $[1]^{+2}$ and $[3]^{+3}$, respectively. $[1]^{+2}$ has a doublet ground state, whereas $[3]^{+3}$ is a triplet biradical (corroborated by DFT; see the Supporting Information). The spin-density plots for these species are given in Figure 10. Despite the fact that the unpaired electron density is more or less delocalized over the entire C≡C−TPA moiety, Table S3 indicates that the distal aryl rings (C9−C21, per Chart S1) take on more of a quinonoidal character than the central aryl ring (C3−C8, per Chart S1) upon oxidation. The C6−N1 distances are barely any different whereas there is a significant contraction (by

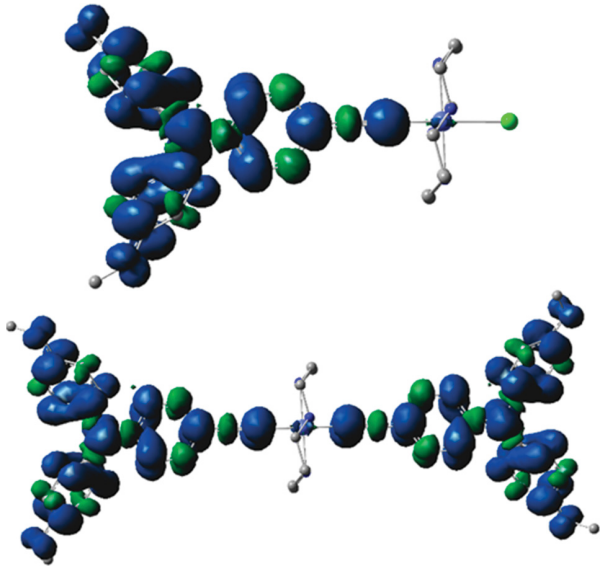

Figure 10. Mulliken spin-density plots for $[1]^{+2}$ (top) and $[3]^{+3}$ (bottom), plotted at lisovaluel = 0.001.

https://dx.doi.org/10.1021/acs.organomet.0c00454
Organometallics 2020, 39, 3250−3259

about 0.02 Å) of the N1−C9 distances in both the oxidized species. This offers preliminary insight into why the spectra of $[\mathbf{1}]^{+2}$ and $[\mathbf{3}]^{+3}$ look similar, and there is likely minimal contribution from the metal d-orbitals to these transitions. The LUMO of both $[\mathbf{1}]^{+}$ and $[\mathbf{3}]^{+}$ are based solely on the Co^{III}(cyclam) unit, reiterating the fact that the first reduction event is localized at the Co center. Ground-state DFT calculations were also carried out on **2a** (Table S8). While there is a sizable contribution from both Co and Cu to the frontier MOs, the π-system of the C≡C−TPA ligand still dominates the valence manifold, just as in the case of $[\mathbf{1}]^{+}$ (Table 4 below). As a result, the Franck−Condon excitations, and by extension the electronic absorption spectra, of **2a** and **2b** are identical to that of [**1**]Cl (Figure S2).

TD-DFT analysis of $[\mathbf{1}]^{+}$, $[\mathbf{1}]^{+2}$, $[\mathbf{3}]^{+}$, and $[\mathbf{3}]^{+3}$ provides insight into the nature of the spectroelectrochemical responses. Since each excited state had contributions from multiple canonical molecular orbitals, natural transition orbitals (NTOs)[42] were calculated for those transitions with the most significant oscillator strengths/extinction coefficients to simplify the picture. The results of these analyses are provided in Figures S10−S17 and Tables S4−S7. While some quantitative differences exist between theory and experiment, there is a general qualitative agreement between them. In the case of $[\mathbf{1}]^{+}$, the most significant transitions lie at energies higher than 28 000 cm^{-1}, all of which are localized within the −C≡C−TPA moiety with no contribution from metal orbitals. The d−d transitions, shown in the inset of Figure 6, are reproduced in the TD-DFT-simulated spectra of $[\mathbf{1}]^{+}$ and $[\mathbf{3}]^{+}$ (17 000−24 000 cm^{-1}, Figures S11 and S15). Since the oscillator strengths of these transitions are very small (f_{oscil} < 0.001), these low-intensity peaks are not discussed further. Upon one-electron oxidation to $[\mathbf{1}]^{+2}$, new spectral features arise that can be divided into five regions (Bands I−V, Figure S13), which are reproduced by TD-DFT calculations. Bands I and II (13 000−14 000 cm^{-1}) are transitions solely based on the −C≡C−TPA part of the molecule from a ligand π-orbital to the now singly occupied orbital with significant $N^{\bullet+}$ character. Band III (ca. 24 000−25 000 cm^{-1}) has some LMCT/MLCT character, with participation from the axial chloro ligand, while band IV (ca. 28 500 cm^{-1}) is once again mainly TPA based, either different $\pi \rightarrow \pi^*$ transitions or others with a small amount of ligand-to-ligand charge transfer (LLCT) character. Band V (ca. 33 000 cm^{-1}) is unique to $[\mathbf{1}]^{+2}$ and has significant contributions from the Co center and the axial chloro ligand.

Both $[\mathbf{3}]^{+}$ and its $2e^{-}$ oxidized ($1e^{-}$ each from the two TPA moieties) derivative, $[\mathbf{3}]^{+3}$, are composed of two symmetric C≡C−TPA axial ligands. As is the case for $[\mathbf{1}]^{+}$ and $[\mathbf{1}]^{+2}$, all the predicted peaks are shifted by roughly 2000 cm^{-1} from the experimental spectra, but the main characteristics of the UV−vis spectra are reproduced by TD-DFT (Figures S14−S17). The NTOs plotted in Tables S6 and S7 show that for both $[\mathbf{3}]^{+}$ and $[\mathbf{3}]^{+3}$ the electronic transitions are localized on these ligands with almost no contribution from the metal center.

CONCLUSION

This work demonstrates synthetic accessibility of both mono- and bis-TPA-acetylide complexes based on Co^{III}(cyclam) and the ability of the former to form η^2-adducts of Cu(I) and Ag(I). Coordination of Cu(I) to the alkyne altered the electronic properties of compound [**1**]Cl, reducing electrochemical reversibility and quenching the observed emission. The electronic absorption spectra of both $[\mathbf{1}]^{+}$ and $[\mathbf{3}]^{+}$ and their respective $1e^{-}$- and $2e^{-}$-oxidized forms were investigated, and the results were analyzed with the aid of TD-DFT analysis. The absorption features are dominated by transitions occurring on the TPA ligand, with the HOMO having significant contributions from the TPA−amino nitrogen lone pair. Upon oxidation, the electron density is delocalized over the TPA moiety to form a radical cation with no contribution from the metal center, resulting in new transitions in the NIR region. The strong spectroscopic features observed herein, suggest that TPA can be leveraged as a spectroscopic tag for future work investigating the electronic properties of metal alkynyl compounds using spectroelectrochemistry. For instance, the electronic coupling between two TPA groups in *trans*-$[Co(MPC)(C_2TPA)_2]^{+}$ is being studied, whereas Co^{III}(MPC) unit (MPC = 5,12-methyl-7,14-phenyl-1,4,8,11-tetraazacyclotetradecane) has been demonstrated to be an efficient mediator for electronic interactions along the axial direction.[43]

EXPERIMENTAL SECTION

Materials. CuCl was purchased from Alfa Aesar. $AgNO_3$ and *n*-butyl lithium were purchased from Sigma-Aldrich. Dry acetonitrile was purchased from ACROS Chemical. All reagents were used as received. $[Co(cyclam)Cl_2]Cl$ was prepared according to literature procedures.[44] Also prepared according to literature procedures was 4-ethynyl-*N*,*N*-bis(4-methoxyphenyl)aniline (HC_2TPA).[36,39] THF was distilled over Na/benzophenone under a N_2 atmosphere. Unless otherwise noted, all reactions were carried out using standard Schlenk techniques under N_2.

Physical Measurements. UV−vis spectra were obtained with a JASCO V-670 spectrophotometer. FT-IR spectra were measured as neat samples using a JASCO FT/IR-6300 spectrometer equipped with a ZnSe ATR accessory. ESI-MS were analyzed on an Advion LC/MS spectrometer. Emission studies were performed on a Varian Cary Eclipse fluorescence spectrophotometer. Fluorescent quantum yields were determined using an anthracene standard. Elemental analysis was carried out by Atlantic Micro Laboratories in Norcross, GA. ^{1}H NMR spectra were recorded on a Varian INOVA300 NMR. Electrochemical analysis was done on a CHI620A voltammetric analyzer with a glassy carbon working electrode (diameter = 2 mm), a Pt-wire auxiliary electrode, and a Ag/AgCl reference electrode; the analyte concentration was 1.0 mM in 4 mL of dry acetonitrile at a 0.1 M *n*-Bu_4NPF_6 electrolyte concentration. Spectrochemical analysis was performed using an OTTLE[40] liquid-sample cell with a 0.2 mm optical path length, 0.3 mL sample volume, and a CaF_2 window procured from F. Hartl (Reading, U.K.). The cell was equipped with a mesh Pt working electrode, a mesh Pt auxiliary electrode, and Ag reference electrode. The analyte concentration was 1.0 mM in 4 mL of dry acetonitrile at a 0.1 M *n*-Bu_4NPF_6 electrolyte concentration.

Synthesis of *trans*-[Co(cyclam)(C_2TPA)Cl]Cl ([1]Cl). $[Co(cyclam)Cl_2]Cl$ (127 mg, 0.35 mmol) was dissolved in 30 mL of MeOH, to which was added 5 mL of a THF solution containing $TPAC_2H$ (77 mg, 0.23 mmol), and the solution was purged with N_2. Upon addition of 0.5 mL of Et_2NH (4.9 mmol) the solution turned turquoise. It was then refluxed for 12 h, resulting in a red solution which was then purified over silica, eluting [**1**]Cl as a dark red band (1:6 $MeCN/CH_2Cl_2$). Recrystallization from MeCN, minimal MeOH, and diethyl ether afforded microcrystalline pink solid. Yield: 0.116 g (0.18 mmol; 75% based on HC_2TPA). ESI-MS $[M^+]$ 622.3 *m*/*z*. UV−vis, λ_{max}/nm (ε/M^{-1} cm^{-1}): 327 (27 200), 410 (820), 513 (300). FT-IR, ν(C≡C)/cm^{-1}: 2114 (w). ^{1}H NMR (300 MHz, CD_3OD) δ 7.23 (d, *J* = 8.8 Hz, 2H), 6.98 (d, *J* = 9.0 Hz, 4H), 6.86 (d, *J* = 9.0 Hz, 4H), 6.75 (d, *J* = 8.7 Hz, 2H), 5.07 (br s, 4H), 3.77 (s, 6H), 2.91 (s, 2H), 2.73−2.64 (m, 8H), 2.56−2.45 (m, 6H), 1.95 (t, *J* = 13.4 Hz, 2H), 1.68−1.58 (m, 2H). Elem. Anal. Found (Calcd) for $C_{35}H_{54}N_6O_{5.5}CoCl_2$ (**1**·2.5H_2O·MeCN·MeOH): C, 54.16 (54.13); H, 7.41(7.01); N, 10.85(10.82).

https://dx.doi.org/10.1021/acs.organomet.0c00454
Organometallics 2020, 39, 3250−3259

Synthesis of *trans*-[Co(cyclam)(C_2TPA-η^2-$CuCl_2$)Cl] (2a). The combination of [**1**]Cl (30 mg, 0.045 mmol) and CuCl (10 mg, 0.05 mmol) in 20 mL of MeCN yielded **2a** after 12 h of refluxing. The precipitate was discarded, and the reaction solution was concentrated via rotary evaporation. The desired product was recrystallized from MeCN with diethyl ether to yield a light pink solid. Yield: 0. 029 g (0.034 mmol; 74% based on **1**). ESI-MS $[M^+]$ 622.1 *m*/*z*. ESI-MS $[CuCl_2]^-$ 132.7 *m*/*z*. UV−vis, λ_{max}/nm (ε/M^{-1} cm^{-1}): 328 (25 200), 410 (1310), 515 (523). FT-IR, ν(C≡C)/cm^{-1}: 2129 (w). ^{1}H NMR (300 MHz, CD_3OD) δ 7.23 (d, *J* = 10.1 Hz, 2H), 6.99 (d, *J* = 9.5 Hz, 4H), 6.86 (d, *J* = 9.3 Hz, 4H), 6.75 (d, *J* = 8.7 Hz, 2H), 5.09 (br s, 4H), 3.78 (s, 6H), 2.82 (s, 2H), 2.70−2.62 (m, 8H), 2.56−2.49 (m, 6H), 1.99−1.90 (m, 2H), 1.86−1.55 (m, 2H). Elem. Anal. Found (Calcd) for $C_{33}H_{49.5}N_{5.5}O_5CoCuCl_3$ (**2a**·3H_2O·0.5MeCN): C, 47.68 (47.63); H, 5.99 (5.99); N, 9.13 (9.26).

Synthesis of *trans*-[Co(cyclam)(C_2TPA-η^2-$Ag(NO_3)_2$)(NO_3)] (2b). In a round-bottomed flask, [**1**]Cl (17 mg, 0.026 mmol) and $AgNO_3$ (18 mg, 0.11 mmol) were stirred at room temperature in 10 mL of MeOH for 4 h. A gray precipitate formed and was filtered out and rinsed until the filtrate ran clear. The filtrate was concentrated. Recrystallization from CH_2Cl_2 and ether afforded **2b** as dark red crystals. Yield: 0.016 g (0.018 mmol; 70% based on [**1**]Cl). ESI-MS $[M^+]$ 649.2 *m*/*z*. ESI-MS $[Ag(NO_3)_2]^-$ 230.7 *m*/*z*. UV−vis, λ_{max}/nm: 326, 410, 519. FT-IR, ν(C≡C)/cm^{-1}: 2030 (w). ^{1}H NMR (300 MHz, CD_3OD) δ 7.21 (br s, 2H), 6.98 (br s, 4H), 6.87 (br s, 4H), 6.76 (br s, 2H), 5.17 (br s, 4H), 3.79 (s, 6H), 3.04−2.93 (m, 4H), 2.90−2.27 (m, 12H), 2.16−1.93 (m, 2H), 2.02−1.48 (m, 2H). Elem. Anal. Found (Calcd) for $C_{33}H_{44}N_8O_{11}CoAgCl_2$ (**2b**·CH_2Cl_2): C, 41.01 (41.01); H, 4.45 (4.59); N, 11.90 (11.59).

Synthesis of *trans*-[Co(cyclam)(C_2TPA)$_2$]Cl ([3]Cl). A solution of LiC_2TPA (prepared from 1.88 mmol of HC_2TPA, 2.5 mmol of *n*-BuLi, and 20 mL of THF) was added to a flask containing [Co(cyclam)Cl_2]Cl (228 mg, 0.63 mmol). Upon addition, the reaction turned from red to dark brown. After 3 h, the reaction was quenched and purified over silica with [**3**]Cl eluting as a dark brown band using 1:5 MeOH/CH_2Cl_2. Recrystallization from CH_2Cl_2 with ether yielded a light brown solid. Yield: 0.501 g (0.53 mmol; 84% based on Co). ESI-MS $[M^+]$ 915.3 *m*/*z*. UV−vis, λ_{max}/nm (ε/M^{-1} cm^{-1}): 333 (47 600), 470 (406). FT-IR, ν(C≡C)/cm^{-1}: 2096 (m). ^{1}H NMR (300 MHz, $CDCl_3$) δ 7.38 (d, *J* = 8.7 Hz, 4H), 7.02 (d, *J* = 9.0 Hz, 8H), 6.86 (d, *J* = 6.9 Hz, 4H), 6.81 (d, *J* = 8.9 Hz, 8H), 4.40 (br s, 4H), 3.79 (s, 12H), 2.93 (s, 2H), 2.86−2.76 (m, 6H), 2.71−2.60 (m, 8H), 1.91−1.86 (m, 2H), 1.65−1.60 (m, 2H). Elem. Anal. Found (Calcd) for $C_{54.5}H_{63}N_6O_5CoCl_2$ (**3**·H_2O·0.5CH_2Cl_2): C, 65.01 (64.69); H, 6.41 (6.27); N, 8.47 (8.30).

Attempted Synthesis of *trans*-[Co(cyclam)(C_2TPA)$_2$]Cl η^2 Complexes. Compound [**3**]Cl was stirred in an acetonitrile solution at room temperature in the presence of excess CuCl or $AgNO_3$ for 6 h. An insoluble yellow precipitate formed that could not be purified or analyzed further. ESI-MS $[M^+]$ analysis of the solution suggested degradation of [**3**]Cl to [**1**]Cl.

X-ray Crystallographic Analysis. Single crystals of compounds [**1**]Cl, **2a**, **2b**, and [**3**]Cl were grown via slow diffusion of diethyl ether into a solution of MeOH/THF (1:1) for [**1**]Cl, **2a**, or **2b** and in a solution of CH_2Cl_2/MeOH (1:1) for [**3**]Cl. X-ray diffraction data was obtained on a Bruker Quest diffractometer with Mo Kα radiation (λ = 0.71073 Å) at 150 K. Data were collected; reflections were indexed and processed using APEX3.[45] The space groups were assigned, and the structures were solved by direct methods using XPREP within the SHELXTL suite of programs[46,47] and refined using Shelxl and Shelxle.[48,49]

■ ASSOCIATED CONTENT

Supporting Information

The Supporting Information is available free of charge at https://pubs.acs.org/doi/10.1021/acs.organomet.0c00454.

(Experimental crystallographic details; normalized emission ([**1**]Cl and [**3**]Cl) and absorption spectra ([**1**]Cl, **2a** and **2b**); Gaussian fit peak analysis for [**1**]Cl and [**3**]Cl; ^{1}H NMR spectra for compounds [**1**]Cl, **2a**, **2b** and [**3**]Cl, and computational details for [**1**]Cl, **2a**, and [**3**]Cl PDF)

Accession Codes

CCDC 2013775−2013778 contain the supplementary crystallographic data for this paper. These data can be obtained free of charge via www.ccdc.cam.ac.uk/data_request/cif, or by emailing data_request@ccdc.cam.ac.uk, or by contacting The Cambridge Crystallographic Data Centre, 12 Union Road, Cambridge CB2 1EZ, UK; fax: +44 1223 336033.

■ AUTHOR INFORMATION

Corresponding Author

Tong Ren − *Department of Chemistry, Purdue University, West Lafayette, Indiana 47907, United States*; Email: tren@purdue.edu

Authors

Susannah D. Banziger − *Department of Chemistry, Purdue University, West Lafayette, Indiana 47907, United States*

Adharsh Raghavan − *Department of Chemistry, Purdue University, West Lafayette, Indiana 47907, United States*

Matthias Zeller − *Department of Chemistry, Purdue University, West Lafayette, Indiana 47907, United States*; orcid.org/0000-0002-3305-852X

Complete contact information is available at: https://pubs.acs.org/10.1021/acs.organomet.0c00454

Notes

The authors declare no competing financial interest.

■ ACKNOWLEDGMENTS

We gratefully acknowledge financial support from the National Science Foundation (CHE 1764347 for research and CHE 1625543 for X-ray diffractometers). We would like to thank Brandon Mash for assistance with X-ray data collection of [**1**]Cl and **2a**. SDB thanks Purdue University for a Cagiantas Fellowship.

■ REFERENCES

(1) Nast, R. Coordination Chemistry of Metal Alkynyl Compounds. *Coord. Chem. Rev.* **1982**, *47*, 89−124.

(2) Bruce, M. I. Transition Metal Complexes Containing Allenylidene, Cumulenylidene, and Related Ligands. *Chem. Rev.* **1998**, *98*, 2797−858.

(3) Bruce, M. I.; Low, P. J. Transition Metal Complexes Containing All-Carbon Ligands. *Adv. Organomet. Chem.* **2004**, *50*, 179−444.

(4) Haque, A.; Al-Balushi, R. A.; Al-Busaidi, I. J.; Khan, M. S.; Raithby, P. R. Rise of Conjugated Poly-ynes and Poly(Metalla-ynes): From Design Through Synthesis to Structure−Property Relationships and Applications. *Chem. Rev.* **2018**, *118*, 8474−8597.

(5) Szafert, S.; Gladysz, J. A. Carbon in One Dimension: Structural Analysis of the Higher Conjugated Polyynes. *Chem. Rev.* **2003**, *103*, 4175−4206.

(6) Szafert, S.; Gladysz, J. A. Update 1 of: Carbon in One Dimension: Structural Analysis of the Higher Conjugated Polyynes. *Chem. Rev.* **2006**, *106*, PR1−PR33.

(7) Ren, T. Diruthenium σ-Alkynyl Compounds: A New Class of Conjugated Organometallics. *Organometallics* **2005**, *24*, 4854−4870.

(8) Launay, J. P. Mixed-Valent Compounds and their Properties - Recent Developments. *Eur. J. Inorg. Chem.* **2020**, *2020*, 329−341.

(9) Gendron, F.; Groizard, T.; Le Guennic, B.; Halet, J. F. Electronic Properties of Poly-Yne Carbon Chains and Derivatives with

Transition Metal End-Groups. *Eur. J. Inorg. Chem.* **2020**, *2020*, 667−681.
(10) Ezquerra, R.; Eaves, S. G.; Bock, S.; Skelton, B. W.; Perez-Murano, F.; Cea, P.; Martin, S.; Low, P. J. New routes to organometallic molecular junctions via a simple thermal processing protocol. *J. Mater. Chem. C* **2019**, *7*, 6630−6640.
(11) Tanaka, Y.; Kato, Y.; Tada, T.; Fujii, S.; Kiguchi, M.; Akita, M. ″Doping″ of Polyyne with an Organometallic Fragment Leads to Highly Conductive Metallapolyyne Molecular Wire. *J. Am. Chem. Soc.* **2018**, *140*, 10080−10084.
(12) Zhu, H.; Pookpanratana, S. J.; Bonevich, J. E.; Natoli, S. N.; Hacker, C. A.; Ren, T.; Suehle, J. S.; Richter, C. A.; Li, Q. Redox-Active Molecular Nanowire Flash Memory for High-Endurance and High-Density Non-Volatile Memory Applications. *ACS Appl. Mater. Interfaces* **2015**, *7*, 27306−27313.
(13) Zhang, L. Y.; Duan, P.; Wang, J. Y.; Zhang, Q. C.; Chen, Z. N. Ruthenium(II) as Conductive Promoter To Alleviate Conductance Attenuation in Oligoynyl Chains. *J. Phys. Chem. C* **2019**, *123*, 5282−5288.
(14) Ko, C.-C.; Yam, V. W.-W. Coordination Compounds with Photochromic Ligands: Ready Tunability and Visible Light-Sensitized Photochromism. *Acc. Chem. Res.* **2018**, *51*, 149−159.
(15) Lang, H.; Jakob, A.; Milde, B. Copper(I) Alkyne and Alkynide Complexes. *Organometallics* **2012**, *31*, 7661−7693.
(16) Gao, L.-B.; Zhang, L.-Y.; Shi, L.-X.; Chen, Z.-N. Syntheses, Characterization, Redox Properties, and Mixed-Valence Chemistry of Tetra- and Hexanuclear Diyndiyl Complexes. *Organometallics* **2005**, *24*, 1678−1684.
(17) Banziger, S. D.; Ren, T. Syntheses, Structures and Bonding of 3d Metal Alkynyl Complexes of Cyclam and Its Derivatives. *J. Organomet. Chem.* **2019**, *885*, 39−48.
(18) Ren, T. A Sustainable Metal Alkynyl Chemistry: 3d Metals and Polyaza Macrocyclic Ligands. *Chem. Commun.* **2016**, *52*, 3271−3279.
(19) Hoffert, W. A.; Kabir, M. K.; Hill, E. A.; Mueller, S. M.; Shores, M. P. Stepwise acetylide ligand substitution for the assembly of ethynylbenzene-linked Co(III) complexes. *Inorg. Chim. Acta* **2012**, *380*, 174−180.
(20) Banziger, S. D.; Cook, T. D.; Natoli, S. N.; Fanwick, P. E.; Ren, T. Synthetic and Structural Studies of Mono-acetylide and Unsymmetric Bis-acetylide Complexes based on CoIII-cyclam. *J. Organomet. Chem.* **2015**, *799*−*800*, 1−6.
(21) Natoli, S. N.; Zeller, M.; Ren, T. An Aerobic Synthetic Approach toward Bis-Alkynyl Cobalt(III) Compounds. *Inorg. Chem.* **2017**, *56*, 10021−10031.
(22) Banziger, S. D.; Li, X.; Valdiviezo, J.; Zeller, M.; Zhang, P.; Beratan, D. N.; Rubtsov, I.; Ren, T. Unsymmetrical Bis-Alkynyl Complexes Based on Co(III)(cyclam): Synthesis, Ultrafast Charge Separation, and Analysis. *Inorg. Chem.* **2019**, *58*, 15487−15497.
(23) Banziger, S. D.; Zeller, M.; Ren, T. New Synthetic Route for Co(III) Dissymmetric Bisalkynyl Complexes Based on Co(III)-(cyclam)(C2NAPMes). *Eur. J. Inorg. Chem.* **2019**, *2019*, 4766−4772.
(24) Lambert, C.; Nöll, G. The Class II/III Transition in Triarylamine Redox Systems. *J. Am. Chem. Soc.* **1999**, *121*, 8434−8442.
(25) Hankache, J.; Wenger, O. S. Organic Mixed Valence. *Chem. Rev.* **2011**, *111*, 5138−5178.
(26) Yang, X. F.; Jin, X. Y.; Zhang, M. X.; Yin, J.; Liu, S. H. Synthesis and properties of contorted hexabenzocoronenes with arylamino groups. *Tetrahedron* **2020**, *76*, 131106.
(27) Zhang, M. X.; Zhang, J.; Yin, J.; Hartl, F.; Liu, S. H. Anodic electrochemistry of mono- and dinuclear aminophenylferrocene and diphenylaminoferrocene complexes. *Dalton Trans.* **2018**, *47*, 6112−6123.
(28) Thakker, P. U.; Aru, R. G.; Sun, C.; Pennington, W. T.; Siegfried, A. M.; Marder, E. C.; Wagenknecht, P. S. Synthesis of trans Bis-alkynyl Complexes of Co(III) Supported by a Tetradentate Macrocyclic Amine: A Spectroscopic, Structural, and Electrochemical Analysis of π-Interactions and Electronic Communication in the CC-M-CC Structural Unit. *Inorg. Chim. Acta* **2014**, *411*, 158−164.
(29) Natoli, S. N.; Zeller, M.; Ren, T. Stepwise Synthesis of Bis-Alkynyl CoIII(cyclam) Complexes under Ambient Conditions. *Inorg. Chem.* **2016**, *55*, 5756−5758.
(30) Mak, T. C. W.; Zhao, X. L.; Wang, Q. M.; Guo, G. C. Synthesis and structural characterization of silver(I) double and multiple salts containing the acetylenediide dianion. *Coord. Chem. Rev.* **2007**, *251*, 2311−2333.
(31) Juvenal, F.; Langlois, A.; Bonnot, A.; Fortin, D.; Harvey, P. D. Luminescent 1D-and 2D-Coordination Polymers Using CuX Salts (X = Cl, Br, I) and a Metal-Containing Dithioether Ligand. *Inorg. Chem.* **2016**, *55*, 11096−11109.
(32) Tsuchida, R. Absorption Spectra of Co-ordination Compounds. I. *Bull. Chem. Soc. Jpn.* **1938**, *13*, 388−400.
(33) Amthor, S.; Noller, B.; Lambert, C. UV/Vis/NIR spectral properties of triarylamines and their corresponding radical cations. *Chem. Phys.* **2005**, *316*, 141−152.
(34) Piechota, E. J.; Troian-Gautier, L.; Sampaio, R. N.; Brennaman, M. K.; Hu, K.; Berlinguette, C. P.; Meyer, G. J. Optical Intramolecular Electron Transfer in Opposite Directions through the Same Bridge That Follows Different Pathways. *J. Am. Chem. Soc.* **2018**, *140*, 7176−7186.
(35) Schnaubelt, L.; Petzold, H.; Dmitrieva, E.; Rosenkranz, M.; Lang, H. A solvent- and temperature-dependent intramolecular equilibrium of diamagnetic and paramagnetic states in Co complexes bearing triaryl amines. *Dalton Trans.* **2018**, *47*, 13180−13189.
(36) Planells, M.; Abate, A.; Hollman, D. J.; Stranks, S. D.; Bharti, V.; Gaur, J.; Mohanty, D.; Chand, S.; Snaith, H. J.; Robertson, N. Diacetylene bridged triphenylamines as hole transport materials for solid state dye sensitized solar cells. *J. Mater. Chem. A* **2013**, *1*, 6949−6960.
(37) Zhang, J.; Guo, S.-Z.; Dong, Y.-B.; Rao, L.; Yin, J.; Yu, G.-A.; Hartl, F.; Liu, S. H. Multistep Oxidation of Diethynyl Oligophenylamine-Bridged Diruthenium and Diiron Complexes. *Inorg. Chem.* **2017**, *56*, 1001−1015.
(38) Judkins, E. C.; Zeller, M.; Ren, T. Synthesis and Characterizations of Macrocyclic Cr(III) and Co(III) 1-Ethynyl Naphthalene and 9-Ethynyl Anthracene Complexes: An Investigation of Structural and Spectroscopic Properties. *Inorg. Chem.* **2018**, *57*, 2249−2259.
(39) Heyer, E.; Ziessel, R. Panchromatic Push-Pull Dyes of Elongated Form from Triphenylamine, Diketopyrrolopyrrole, and Tetracyanobutadiene Modules. *Synlett* **2015**, *26*, 2109−2116.
(40) Krejcik, M.; Danek, M.; Hartl, F. Simple construction of an infrared optically transparent thin-layer electrochemical cell: Applications to the redox reactions of ferrocene, Mn2(CO)10 and Mn(CO)3(3,5-di-t-butyl-catecholate)-. *J. Electroanal. Chem. Interfacial Electrochem.* **1991**, *317*, 179−187.
(41) Dapperheld, S.; Steckhan, E.; Brinkhaus, K.-H. G.; Esch, T. Organic Electron Transfer Systems, II Substituted Triarylamine Cation-Radical Redox Systems - Synthesis, Electrochemical and Spectroscopic Properties, Hammet Behavior, and Suitability as Redox Catalysts. *Chem. Ber.* **1991**, *124*, 2557−2567.
(42) Martin, R. L. Natural Transition Orbitals. *J. Chem. Phys.* **2003**, *118*, 4775−4777.
(43) Mash, B. L.; Yang, Y.; Ren, T. Improving Redox Reversibility and Intermetallic Coupling of Co(III) Alkynyls through Tuning of Frontier Orbitals. *Organometallics* **2020**, *39*, 2019−2025.
(44) Bosnich, B.; Tobe, M. L.; Webb, G. A. Complexes of Nickel(2) with a Cyclic Tetradentate Secondary Amine. *Inorg. Chem.* **1965**, *4*, 1109−1112.
(45) *APEX3* v2016.9−0, *Saint* v8.34A, *Saint* v8.37A; Bruker AXS, Inc.: Madison, WI, 2016.
(46) *SHELXTL suite of programs*, version 6.14; Bruker AXS Inc.: Madison, WI, 2003.
(47) Sheldrick, G. M. A short history of SHELX. *Acta Crystallogr., Sect. A: Found. Crystallogr.* **2008**, *64*, 112−122.
(48) Sheldrick, G. M. Crystal structure refinement with SHELXL. *Acta Crystallogr., Sect. C: Struct. Chem.* **2015**, *71*, 3−8.

https://dx.doi.org/10.1021/acs.organomet.0c00454
Organometallics 2020, 39, 3250−3259

(49) Hübschle, C. B.; Sheldrick, G. M.; Dittrich, B. ShelXle: a Qt graphical user interface for SHELXL. *J. Appl. Crystallogr.* **2011**, *44*, 1281−1284.

https://dx.doi.org/10.1021/acs.organomet.0c00454
Organometallics 2020, 39, 3250−3259